Nanoscale

FULL PAPER

Promoter Effect of Hydration on the Nucleation of Nanoparticles: Direct Observation for Gold and Copper on Rutile TiO_2 (110)†

(Electronic Supplementary Information)

Mathilde Iachella,[a] Axel Wilson,[b,c] Ahmed Naitabdi,[b] Romain Bernard,[b] Geoffroy Prévot,[b] and David Loffreda*[a]

1 Experiments

1.1 Identification of Oxygen Vacancies and Hydroxyl Groups on a Highly Reduced TiO_2 Surface

In the following Figure S1, the way the oxygen vacancies and hydroxyl groups are identified on the STM images is recalled. Further details regarding the identification of water based adsorbates can be found in Ref.[1].

1.2 Nucleation of Au Nanoparticles on a Partially Hydrated and Reduced TiO_2 Surface

Figure S2 shows a sequence of images acquired over 30 minutes in the same area of the sample, before Au evaporation (see Figures 1 and 2 of the manuscript for comparison of the surface before and after evaporation). A careful comparison of the images shows that the mobility of OH groups is rather small: during the time needed for the acquisition of two successive images (5 minutes), less than 1% of OH have jumped from one site to the next one along the [001] direction of TiO_2. In particular, we observe that O_v can be covered by OH groups. During the whole acquisition (30 min), no movement of O_v, which cover around 5% of the surface area, is registered.

1.3 Nucleation of Au Nanoparticles on a More Reduced TiO_2 Sample Surface

In a specific experiment, a highly reduced surface composed of long TiO_x stripes is prepared. The OH groups cover around 15% of the clean surface unit cells and are gathered in domains separated by small areas of reduced TiO_2 (see Figure S3). Approximately 0.03 ML of Au is deposited on the surface which roughly corresponds to three times the amount deposited on the surface presented in Figures 1 and 2 of the manuscript. The subtraction of the drift corrected images in Figures S3 (a) and (b) is then superimposed to the clean surface in Figure S3 (c) to identify the nucleation sites of the NPs. The experiment shows that a vast majority of NPs grows on the reduced TiO_2 surface free from OH groups and on TiO_x stripes. Additionally, blue arrows in Figure S3 (c) show that the shape of the NPs growing close to a hydrated region can be modified by the presence of hydroxyl groups. The quasi absence of NP nucleation over OH areas causes the diffusion toward the reduced TiO_2 surface of Au atoms deposited on this region during growth. Note that the OH domains remain visible after deposition. Hence, the probability to find an Au atom at the periphery of hydroxyl regions during growth is larger than that on the rest of the surface.

1.4 Nucleation of Cu Nanoparticles on a Partially Hydrated and Reduced TiO_2 Surface

For this experiment, due to a chemical or morphological change of the tip end between the two images, the appearance of O_v and OH groups has changed. This change occurs before Cu evaporation, as shown in Figures S4 (a) and (b). The difference between two consecutive images performed on the same are with a different tip termination shows that the difference between the two images is mainly due to a lower contrast between the bridging oxygen and the Ti 5f rows (Figure S4 (e)). After Cu evaporation, the difference between images acquired prior and after evaporation (Figure S4 (f)) allows us to determine the nucleation sites of the Cu nanoparticles.

A comparison between the nucleation statistics for Au and Cu NPs is shown under the shape of pie charts in the in Figure S5.

2 Methodology

2.1 Computational Details

Calculations have been performed by using density functional theory (DFT) in periodic boundary conditions, with the Vienna *ab-initio* simulation package (VASP[2–4]). The generalized gradient approximation (GGA) has been used with the Perdew-Burke-Ernzerhof exchange-correlation functional (PBE[5]), and the projector augmented-wave method (PAW[6]). Dispersion effects have been evaluated by using the Grimme's zero damping DFT-D3 (D3(0)) model[7]. An energy cut-off of 400 eV has been consid-

[a] *Univ Lyon, Ens de Lyon, CNRS UMR 5182, Université Claude Bernard Lyon 1, Laboratoire de Chimie, F-69342, Lyon, France. Fax: +33.4.72.72.88.60; Tel: +33.4.72.72.88.43; E-mail: david.loffreda@ens-lyon.fr*
[b] *Institut des NanoSciences de Paris, UMR CNRS 7588, Université Pierre et Marie Curie-Paris 6, 4, Place Jussieu, 75005 Paris, France.*
[c] *Synchrotron SOLEIL, L'Orme des Merisiers, Saint-Aubin, 91192 Gif-sur-Yvette cedex, France.*

ered for the expansion of the plane-wave basis set. Spin-polarized calculations have been performed throughout the study. Accurate geometry optimizations have been ensured by tight criteria for the convergence of total electronic energy (10^{-7} eV) and for the residual forces acting on the nuclei (-0.01 eV/Å^{-1}).

The theoretical description of rutile TiO_2 (110) stoichiometric and reduced non-polar surfaces leads to two main issues[8]. First, the band gap width is underestimated (1.7 eV with GGA-PBE *vs* 3.05 eV experimentally). Second, for reduced TiO_2 surfaces, *i.e.* surfaces exhibiting oxygen vacancies, two electrons are released back to the oxide surface per removed oxygen atom. The formation of oxygen vacancies creates an electronic state in the TiO_2 gap, the so-called gap state (lying 2.3 eV above the valence band and 0.7 eV below the conduction band[9], hence at $3/4$ of the band gap). The usual GGA functionals fail to describe the corresponding electron localization at a metallic center. A probative semi-empirical approach, namely DFT+U, has been proposed to improve this spurious delocalization. An additional term U, corresponding to electron on-site repulsion and based on a Hubbard model is considered to cure the self-interaction error. In this study, the Dudarev's approach (PBE+U) has been selected[10] with an optimal value U_{eff} of 4.2 eV, offering the best compromise between the opening of the band gap (2.16 eV) and the localization of the gap state (at $3/5$ of the band gap)[8].

TiO_2 rutile bulk is a quadratical crystal where $a = b \neq c$ and $\alpha = \beta = \gamma = 90^{\text{o}}$. Our PBE+$U$ results (with a Monkhorst-Pack[11] k-points mesh of $(9 \times 9 \times 15)$, corresponding to 120 irreducible points) are in fair agreement with experimental measurements[12]: $a_{\text{theo}} = 4.615$ Å, $a_{\text{exp}} = 4.593$ Å; $c_{\text{theo}} = 3.001$ Å, $c_{\text{exp}} = 2.958$ Å and $u_{\text{theo}} = 0.304$, $u_{\text{exp}} = 0.305$. The systematic error on the band gap has been evaluated by changing the extension of the Ti atom valence ($3d^3 4s^1$ *vs* $3s^2 3p^6 3d^3 4s^1$), the pseudopotentials (PAW-PBE *vs* GW) and the choice of the non-local dispersion corrected functional (vdWDF2 and BEEF-vdW). The value varies from 2.16 eV (PBE+U, 4 valence electrons) to 2.33 eV (PBE+U, 12 valence electrons), to 1.75 eV (BEEF-vdW, 12 valence electrons), to 2.2 eV (vdWDF2, 12 valence electrons) and to 2.35 eV (PBE+U with GW pseudopotentials, 12 valence electrons). The optimal lattice parameters are weakly perturbed by the change of the functional, the valence or the pseudopotentials. According to our tests, the inclusion of dispersion makes worse the prediction of the band gap (see also the conclusions of a previous theoretical work[13]), whereas GW pseudopotentials agree quantitatively with PAW-PBE pseudopotentials. In addition, the extension of the valence up to 12 electrons offers the best prediction for the band gap. Hence, for all the study, we have chosen PBE+U, PBE-PAW and 12 valence electrons for Ti atoms. The numeric error has been estimated by changing the k-points grids and corresponding number of irreducible points. A convergence on the total electronic energy of $\pm 2.10^{-4}$ eV is ensured by a $(9 \times 9 \times 15)$ mesh.

2.2 Surface Models

Various surfaces of TiO_2 (110) have been modeled in this work (cf. Figure S6). The stoichiometric non-polar termination is presented in Figure S6 (a) and (b). It is described by a (2×1) supercell and is terminated by bridging oxygen rows along c. A reduced termination has been considered with a single oxygen vacancy located in the surface (see Figures S6 (c) and (d)). The reduced surface is described by a (3×1) supercell (corresponding to a vacancy surface coverage of $1/3$ ML). The vacuum space between two equivalent slabs along the z direction is set to 20 Å. In all those surface models, one oxide layer contains 3 atomic planes (following the sequence O-Ti_2O_2-O). The associated k-points grids are defined from the bulk rule and thus are chosen as $(7\times7\times1)$ and $(5\times7\times1)$ for stoichiometric and reduced surfaces, respectively. One important characteristic of the surface models is the choice of the thickness of the symmetric slab based on the convergence of the surface energy. A detailed analysis of surface energy calculations for stoichiometric surface model as a function of the slab thickness shows that absolute convergence is obtained for a 13-layer thick slab (593 mJ.m^{-2}). This been said, a compromise is done to make the theoretical study possible by keeping 7-layer thick slab (leading to a systematic error of 70 mJ.m^{-2}). For the two models of reduced surfaces, the convergence of the surface energy is more difficult, where more than 13-layer thick symmetric slabs are required to reach an equivalent accuracy. This delicate question is rarely mentioned in the literature. For a sake of consistency with stoichiometric surfaces, 7-layer thick slabs represent our converged models. The surface energies for the reduced surfaces are 1109 and 1331 mJ.m^{-2} with a single oxygen vacancy in the surface and sub-surface layer, respectively. As a conclusion, the presence of a vacancy in the sub-surface is possible but much less favorable than in the surface.

Regarding adsorption properties of Au and Cu on those TiO_2 surfaces, non-symmetric slabs composed of 4 layers or 12 atomic planes (equivalent to 7-layer thick symmetric slab) are built up. These adsorptions are considered both on stoichiometric and reduced TiO_2 surfaces with associated supercells of (2×1), (3×1) and corresponding coverage θ_M of $1/4$ ML, $1/6$ ML, respectively. In the geometry optimizations, the bottommost oxide layer is frozen to the bulk-like optimal structure, while the 3 uppermost layers are allowed to relax completely.

The hydration of the support with or without one coadsorbed metallic atom is considered by adsorbing dissociatively several water molecules (H + OH). The dissociation can occur either on the TiO_2 support or on the metallic adsorbate (if present), leading in this latter case to a grafted hydroxylated organometallic complex. The hydration coverage θ^M_{hyd} depends on the presence of the metal M. In all the cases (with or without the metal, stoichiometric or reduced surfaces), it is varied in the range 0-1 ML. In presence of Au or Cu, the saturation corresponds to 4 and 5 dissociatively adsorbed water molecules, for the stoichiometric and reduced surfaces, respectively. Without the metallic coadsorbate, the saturation is reached by adsorbing dissociatively 2 and 3 water molecules, for the stoichiometric and reduced surfaces, respectively.

In all the DFT models of clean TiO_2 surfaces and of adsorbed systems, VASP is allowed to relax the spin-polarization simultaneously with the geometry optimizations. For converged results, the spin-polarization is essentially held by the Ti atoms of the

surface layers (never on the Au or Cu atoms). Tests imposing the spin-polarization to small integer values (ranging from 0 to 3) are performed on the optimized structures to check whether the direct minimization had led to the most stable magnetic state. By following such a procedure, we have never registered a more stable spin-polarized state as the one obtained by VASP.

2.3 Adsorption and Hydration Energetics

In order to evaluate the adsorption strength for the metallic atoms and water on the various supports, we have introduced several definitions of the adsorption, hydration and coadsorption energies, reported in Table 1 of the manuscript. First, the adsorption energy of a metallic atom has been calculated as follows:

$$E_{ads}^{M/\mathrm{TiO_2}} = E_{M/\mathrm{TiO_2}} - E_{\mathrm{TiO_2}} - E_M \quad (1)$$

Where $E_{M/\mathrm{TiO_2}}$ is the total electronic energy of the adsorbed metallic atom on the stoichiometric or reduced TiO_2, $E_{\mathrm{TiO_2}}$ the total electronic energy of the corresponding TiO_2 slab and E_M the total electronic energy of a metallic atom in vacuum. The total hydration energy of the TiO_2 surfaces reads:

$$E_{hyd}^{n\mathrm{H_2O/TiO_2}} = E_{n\mathrm{H_2O/TiO_2}} - E_{\mathrm{TiO_2}} - nE_{\mathrm{H_2O}} \quad (2)$$

Where $E_{n\mathrm{H_2O/TiO_2}}$ is the total electronic energy of n dissociatively coadsorbed water molecules on the stoichiometric or reduced TiO_2 and $E_{\mathrm{H_2O}}$ the total electronic energy of a water molecule in vacuum. The coadsorption energy of n water molecules and a metallic atom is calculated as follows:

$$E_{coads}^{M,n\mathrm{H_2O/TiO_2}} = E_{M,n\mathrm{H_2O/TiO_2}} - E_{\mathrm{TiO_2}} - nE_{\mathrm{H_2O}} - E_M \quad (3)$$

Where $E_{M,n\mathrm{H_2O/TiO_2}}$ is the total electronic energy of n dissociatively water molecule coadsorbed with a metallic atom on the stoichiometric or reduced TiO_2. The two following equations evaluate the adsorption energy of a metallic atom on a hydrated TiO_2 (110) surface ($E_{ads}^{M/(n\mathrm{H_2O/TiO_2})}$) and the hydration energy of a TiO_2 (110) surface precovered by a metallic atom ($E_{hyd}^{n\mathrm{H_2O}/(M/\mathrm{TiO_2})}$):

$$E_{ads}^{M/(n\mathrm{H_2O/TiO_2})} = E_{M,n\mathrm{H_2O/TiO_2}} - E_{n\mathrm{H_2O/TiO_2}} - E_M \quad (4)$$

$$E_{hyd}^{n\mathrm{H_2O}/(M/\mathrm{TiO_2})} = E_{M,n\mathrm{H_2O/TiO_2}} - E_{M/\mathrm{TiO_2}} - nE_{\mathrm{H_2O}} \quad (5)$$

The energetic balance between the coadsorption energy and the adsorption of the metal and the hydration energy defines the interaction energy between all those coadsorbates (dissociated water molecules and metallic atom):

$$E_{int}^{M-n\mathrm{H_2O}} = E_{coads}^{M,n\mathrm{H_2O/TiO_2}} - E_{hyd}^{n\mathrm{H_2O/TiO_2}} - E_{ads}^{M/\mathrm{TiO_2}} \quad (6)$$

In Table 1 of the manuscript, we report the adsorption energy of Au in presence $E_{ads}^{M/(n\mathrm{H_2O/TiO_2})}$ and absence $E_{ads}^{M/\mathrm{TiO_2}}$ of water, the hydration energy of the bare $E_{hyd}^{n\mathrm{H_2O/TiO_2}}$ and of the Au precovered support $E_{hyd}^{n\mathrm{H_2O}/(M/\mathrm{TiO_2})}$, the coadsorption energy of Au with one and two water molecules $E_{coads}^{M,n\mathrm{H_2O/TiO_2}}$, and the interaction energy between all the coadsorbates $E_{int}^{M-n\mathrm{H_2O}}$.

Our DFT+U calculations have been compared with previous theoretical studies. The publications devoted to the study of the adsorption of Au atom on stoichiometric and reduced non-hydrated surfaces can be classified in three groups. The first group is composed of DFT models performed within the GGA framework with Dacapo and GPAW computational codes[14–16] (restricted formalism, no Hubbard term, no spin-polarization).Their results show that the adsorption on the stoichiometric surface (from -0.35 to -0.6 eV) is weaker than that on the reduced support (from -0.95 to -1.31 eV). The large variability of the corresponding values makes it difficult to select a particular reference. In the second group, GGA-PBE and PAW calculations are performed with VASP package by two different teams[17,18] (restricted formalism, no Hubbard term, no spin-polarization). Their results are in good agreement for both adsorption of Au on the stoichiometric (from -0.34 to -0.22 eV) and reduced (from -2.2 to -2.54 eV) surfaces. The third group of values is generated with spin-unrestricted PBE+U and the Quantum Espresso package (Van der Bilt pseudopotentials)[19]. The related results (-0.58 eV for the adsorption on the stoichiometric surface and -1.54 eV on the reduced one) are in fair agreement with those of the second group (VASP users). Hence the DFT values provided by the last two groups (different methodology, different codes and authors) disagree with those proposed by the first group of articles (same authors, same code). The major point of disagreement concerns the adsorption on the reduced bare surface (the maximum deviation being in the range -0.95, -2.54 eV). Our DFT+U results agree with the second and the third groups (-42 and -213 kJ.mol^{-1} for stoichiometric and reduced surface, respectively).

Besides, a publication by Matthey et *al*. suggests that the adsorption energy decreases from the bare to the hydrated support (from -0.6 to -0.54 eV, respectively).[14] In this study, we offer the opposite trend with an increase of the adsorption strength (from -42 to -64 or -108 kJ.mol^{-1}, depending on the hydration rate).

In the case of Cu adsorption on the non-hydrated stoichiometric and reduced surfaces, there are fewer available results in the state of the art. For the adsorption on stoichiometric surfaces, the previously published values within the GGA framework are surprisingly large (-2.75 eV at the PBE+U level[20] and -2.39 eV at the PW91 level[21]). On the reduced support, there is only one reported value (-1.92 eV at the PBE+U level[20]). Our results are in clear disagreement at two different levels. We show an opposite trend from the stoichiometric (-149 kJ.mol^{-1}) to the reduced (-161 kJ.mol^{-1}) surfaces with a moderate gain of adsorption strength. Moreover, our adsorption energy on the stoichiometric surface is considerably weaker than those in previous reports.

2.4 Gibbs Free Energy Calculations

In order to determine the most stable coadsorption phase $\left((OH+H)_{N_{H_2O}}+M\right)_{(coads)}/TiO_2(\xi)$ between metal M and water (OH + H), in the experimental conditions (as a function of temperature T and the presence of a single surface vacancy ξ), we have evaluated the Gibbs free coadsorption energy related to the

$$N_{H_2O}\ H_2O_{(gas)} + M_{(gas)} + TiO_2(Sto) \rightarrow \left((OH+H)_{N_{H_2O}} + M\right)_{(coads)} / TiO_2(\xi) + \frac{\xi}{2}\ O_{2(gas)} \quad (7)$$

The Gibbs free energy of reactive coadsorption (ΔG_{rcoads}) per unit cell area $\mathscr{A}$ is defined by the following equation, where the gas phase (mixture of H_2O and O_2) plays the role of a reservoir in equilibrium with the coadsobed phase:

$$\Delta G_{rcoads} = \left(\Delta E_{rcoads} - k_B T \ln\left(\left(\frac{P_{O_2}}{k_B T\ Z^0_{trs,O_2}\ Z_{rot,O_2}}\right)^{-\frac{\xi}{2}} \left(\frac{P_{H_2O}}{k_B T\ Z^0_{trs,H_2O}\ Z_{rot,H_2O}}\right)^{N_{H_2O}}\right)\right) / \mathscr{A} \quad (8)$$

Where ΔE_{rcoads} is the reactive coadsorption energy obtained by the difference between the total electronic energy of the coadsorbed system and those of the clean stoichiometric TiO_2 surface and gas phase references (including the totel electronic energy of the metallic atom in vacuum). Z^0_{trs,O_2} and Z^0_{trs,H_2O} are the 3D translational partition functions for the gas phase water and oxygen references. In this formulation, Z^0 means that it depends only on the temperature. Z_{rot,O_2} and Z_{rot,H_2O} are the rotational partition functions of the gas phase molecules. The vibrational entropy contribution is neglected here as a first approximation. In fact, we have evaluated them previously for other oxide[22] or metal[23] catalysts and they don't change the conclusions coming from total electronic energies, in a range of low temperatures (0-400 K). P_{O_2} and P_{H_2O} are the partial pressure of the gas phases.

2.5 Dispersion Effects

In the following section, we expose our DFT results for the adsorption of Au and Cu atoms on stoichiometric, non-hydrated and hydrated TiO_2 (110) surface, considering van der Waals forces (dispersion). To do so, Grimme's zero damping DFT-D3 (D3(0)) semi-empirical model has been used to recalculate the adsorption and coadsorption energetics of relaxed structures for Au, Cu and water on the oxide support (see Table S1). This means that UGGA+U and DFT-D3(0) models have been combined. In Table S1, the values at the UGGA+U level of Table 1 of the manuscript have been also recalled for comparison. For the adsorption on the non-hydrated support, the change of adsorption energy for Au due to dispersion effects is rather weak (-13 kJ.mol^{-1}), while it is almost negligible for Cu (+1 kJ.mol^{-1}). On the hydrated support, van der Waals contributions are weakly stabilizing the adsorption of Au (-9 kJ.mol^{-1}), whereas they have no impact on Cu adsorption. The dispersion effects globally tend to destabilize water on the support in absence of the metal (16−29 kJ.mol^{-1}), but also in its presence (15−34 kJ.mol^{-1}). The coadsorption energy between the metal and water is also systematically weakened (4−31 to kJ.mol^{-1}), while the interaction energy between these two compounds is either slightly decreased for Au and water, or kept constant for Cu and water. In summary, dispersion forces do not modify our conclusions drawn from the UPBE+U method.

References

1 X. Cui, Z. Wang, S. Tan, B. Wang, J. Yang and J. G. Hou, *J. Phys. Chem. C*, 2009, **113**, 13204–13208.
2 G. Kresse and J. Hafner, *Phys. Rev. B*, 1993, **47**, 558.
3 G. Kresse and J. Furthmüller, *Comput. Mater. Sci.*, 1996, **6**, 15.
4 G. Kresse and J. Furthmüller, *Phys. Rev. B*, 1996, **54**, 11169.
5 J. P. Perdew, K. Burke and M. Ernzerhof, *Phys. Rev. Lett.*, 1996, **77**, 3865.
6 G. Kresse and D. Joubert, *Phys. Rev. B*, 1999, **59**, 1758.
7 S. Grimme, J. Antony, S. Ehrlich and H. Krieg, *J. Chem. Phys.*, 2010, **132**, 154104.1–154104.19.
8 B. J. Morgan and G. W. Watson, *Surf. Sci.*, 2007, **601**, 5034–5041.
9 V. E. Henrich, G. Dresselhaus and H. J. Zeiger, *Bulletin of the American Physical Society*, 1976, **21**, 940–941.
10 S. L. Dudarev, G. A. Botton, S. Y. Savrasov, C. J. Humphreys and A. P. Sutton, *Phys. Rev. B*, 1998, **57**, 1505–1509.
11 H. J. Monkhorst and J. D. Pack, *Phys. Rev. B*, 1976, **13**, 5188–5192.
12 P. Vinet, J. Ferrante, J. R. Smith and J. H. Rose, *J. Phys. C Solid State Physics*, 1986, **19**, L467–L473.
13 N. Kumar, P. R. C. Kent, D. J. Wesolowski and J. D. Kubicki, *J. Phys. Chem. C*, 2013, **117**, 23638–23644.
14 D. Matthey, J. G. Wang, S. Wendt, J. Matthiesen, R. Schaub, E. Laegsgaard, B. Hammer and F. Besenbacher, *Science*, 2007, **315**, 1692–1696.
15 G. K. H. Madsen and B. Hammer, *J. Chem. Phys.*, 2009, **130**, 044704.
16 U. Martinez and B. Hammer, *J. Chem. Phys.*, 2011, **134**, 194703.
17 H. Iddir, S. Ogut, N. D. Browning and M. M. Disko, *Phys. Rev. B*, 2005, **72**, 081407.
18 T. Pabisiak and A. Kiejna, *Surf. Sci.*, 2011, **605**, 668–674.
19 M. F. Camellone, P. M. Kowalski and D. Marx, *Phys. Rev. B*, 2011, **84**, 035413.
20 Y. Cai, Z. Bai, S. Chintalapati, Q. Zeng and Y. P. Feng, *J. Chem.*

Phys., 2013, **138**, 154711.
21 L. Giordano, G. Pacchioni, T. Bredow and J. F. Sanz, *Surf. Sci.*, 2001, **471**, 21–31.
22 H. Petitjean, H. Guesmi, H. Lauron-Pernot, G. Costentin, D. Loffreda, P. Sautet and F. Delbecq, *ACS Catal.*, 2014, **4**, 4004–4014.
23 F. Vigné, J. Haubrich, D. Loffreda, P. Sautet and F. Delbecq, *J. Catal.*, 2010, **275**, 129–139.

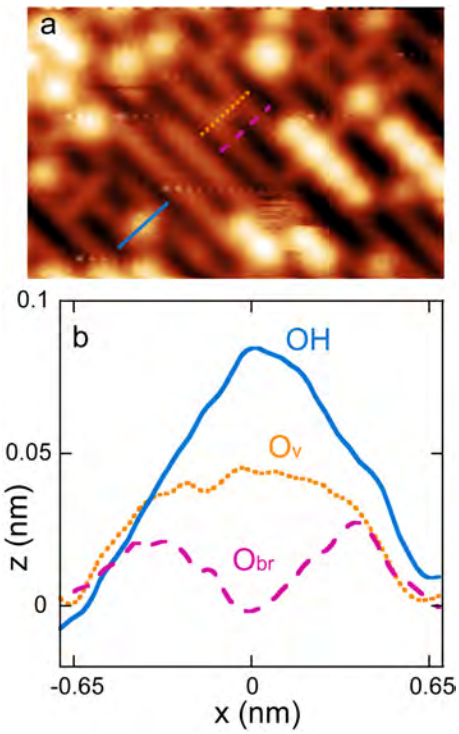

Figure S 1 (a) Partially hydrated and reduced TiO_2 (110) surface before Au evaporation (size of the STM image: 9.2 × 5.3 nm^2). (b) Height profiles along the lines shown in (a). The blue continuous line means "across an hydroxyl group OH", orange dotted line meaning "across an oxygen vacancy O_v" and purple dashed line, "across a regular oxygen bridging atom O_{br}".

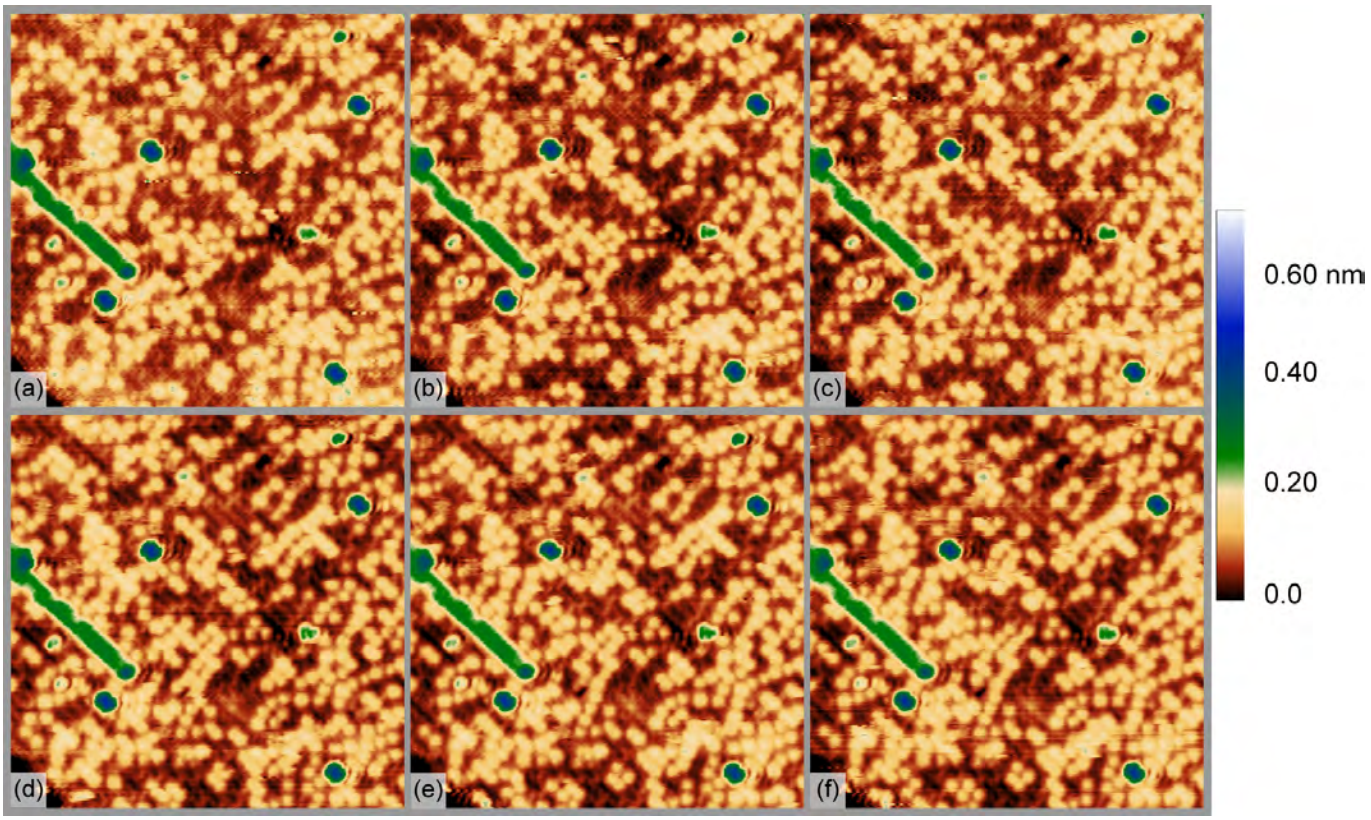

Figure S 2 Size of the STM images: 21 × 21 nm^2. (a) to (f) Sequence of STM images acquired over 30 minutes in the same area of the TiO_2 (110) sample, before Au evaporation. The images have been acquired at times (a) 0, (b) 10 min, (c) 15 min, (d) 20 min, (e) 25 min and (f) 30 min.

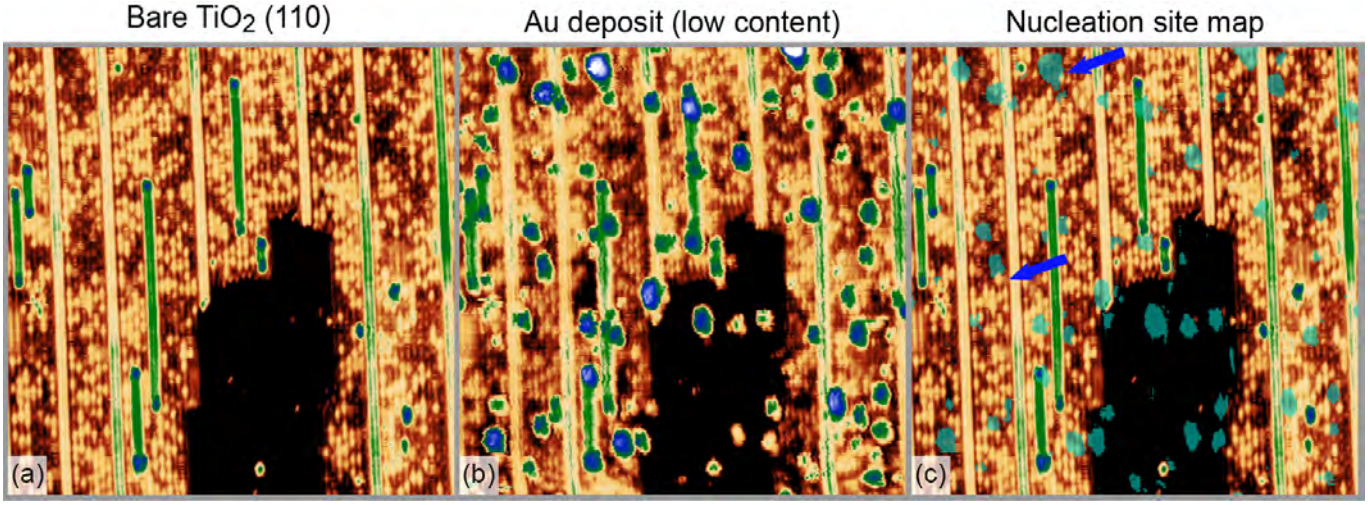

Figure S 3 Size of the STM images: 52 $\times$ 52 nm^2. (a) Clean surface of rutile TiO_2 (110). (b) Same area than (a) after deposition of 3% ML of Au, tip retracted. (c) Position of the nanoparticles determined from (b) (green spots) on the clean surface. The blue arrow points toward NPs of which the shape has been modelled by clustered hydroxyl groups.

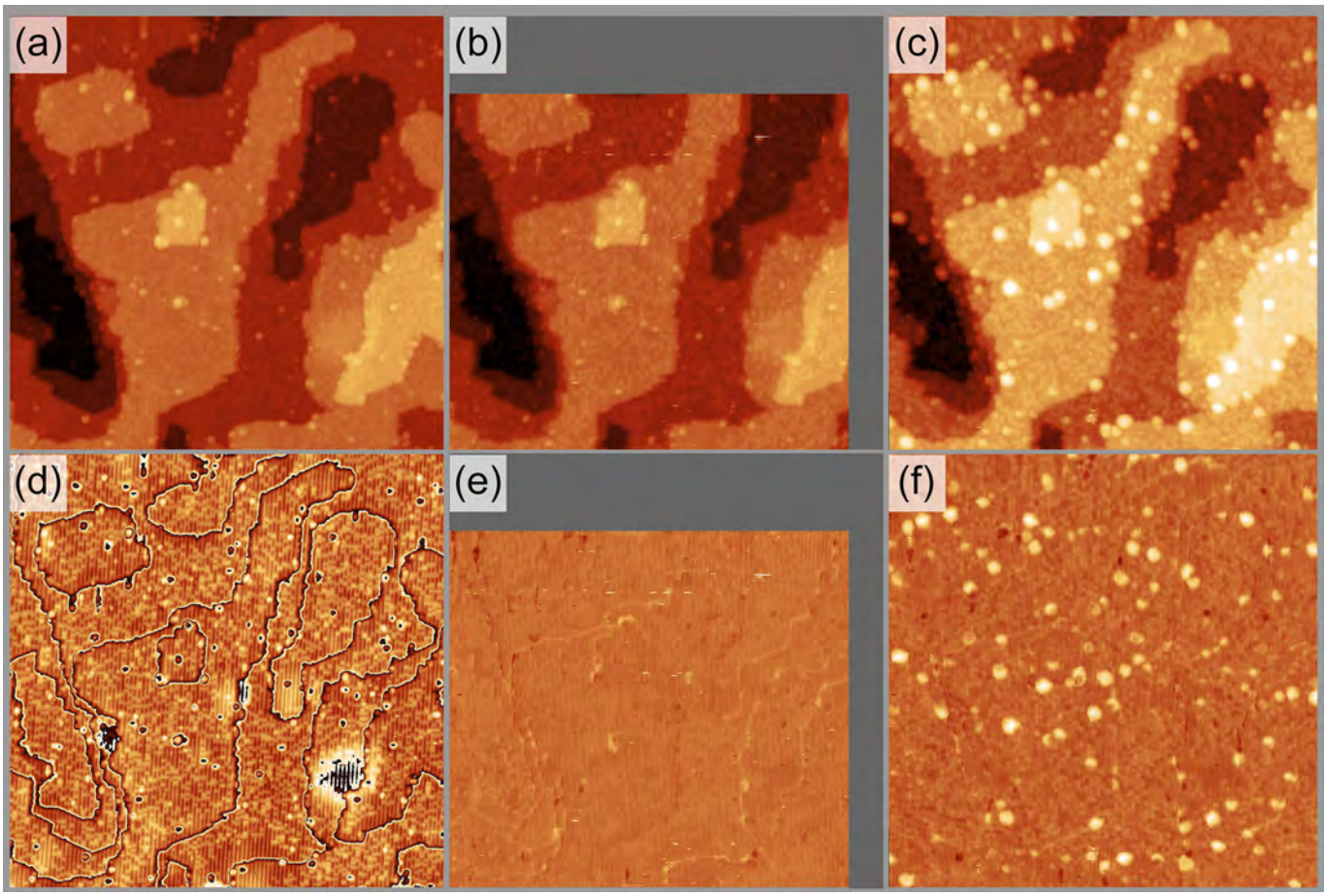

Figure S 4 Evolution of the partially hydrated and reduced TiO_2 (110) surface during Cu evaporation at room temperature (same area in each image). Size of the STM images: 68 $\times$ 68 nm^2. Tunneling conditions: 2V - 0.02 nA. (a) and (b) before Cu evaporation, with a different tip termination, (c) after evaporation of a low amount of Cu (<1 % ML), (d) same as (a) modulo the step height, (e) difference between images (b) and (a), (f) difference between images (c) and (a).

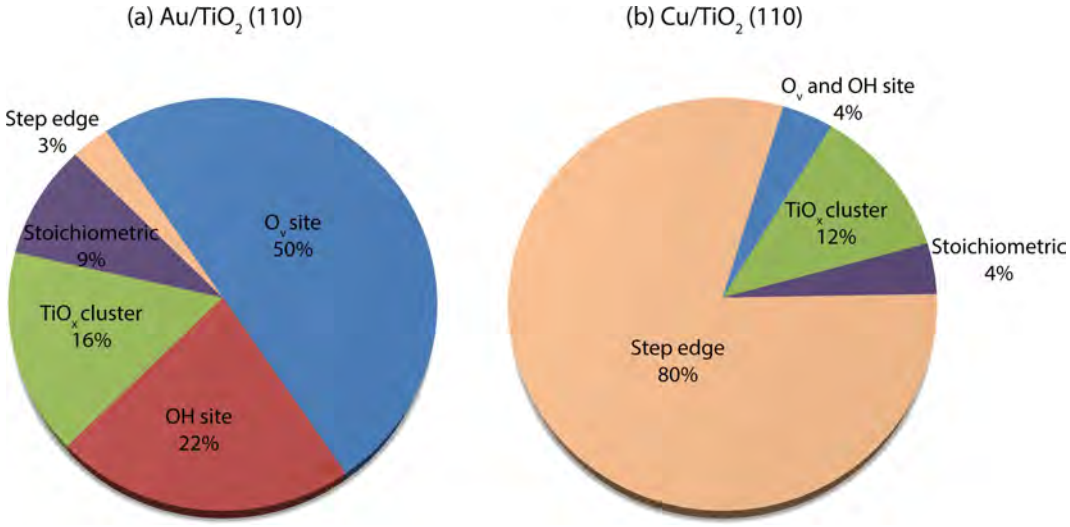

Figure S 5 Pie-charts of the (a) Au and (b) Cu nucleation probabilities on the different sites of the TiO_2 (110) surface.

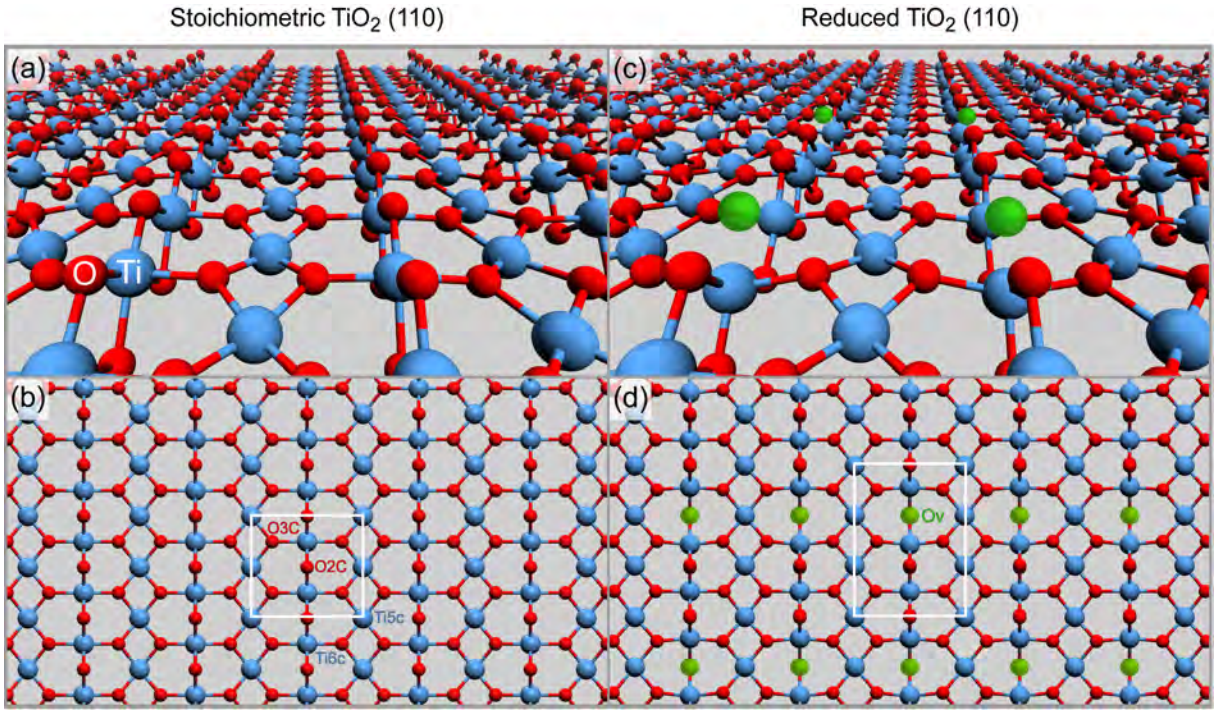

Figure S 6 Lateral and top views of bare stoichiometric ((a) and (b)) and reduced ((c) and (d)) bare TiO_2 (110) surfaces. The definitions of the supercells ((2×1) for stoichiometric termination and (3×1) for reduced surface) appear with white rectangles in (b) and (d). Single oxygen vacancies (O_v) at the surface of the support, along the terminal bridging oxygen rows, are considered and depicted with green spheres.

($kJ.mol^{-1}$)	Stoichiometric TiO_2 (110)				Stoichiometric TiO_2 (110)			
method	UPBE+U				UPBE+U+D3			
non-hydrated	Au		Cu		Au		Cu	
E_{ads}^{M/TiO_2}	-42		-149		-55		-148	
hydrated	Au		Cu		Au		Cu	
	1 H_2O	2 H_2O	1 H_2O	2 H_2O	1 H_2O	2 H_2O	1 H_2O	2 H_2O
$E_{ads}^{M/(nH_2O/TiO_2)}$	-64	-108	-142	-125	-75	-117	-142	-125
$E_{hyd}^{nH_2O/TiO_2}$	-69	-152	-69	-152	-53	-121	-53	-121
$E_{hyd}^{nH_2O/(M/TiO_2)}$	-91	-217	-62	-128	-74	-183	-47	-99
$E_{coads}^{M,nH_2O/TiO_2}$	-133	-259	-211	-277	-129	-238	-195	-246
$E_{int}^{M-nH_2O}$	-22	-66	+6	+23	-20	-62	+6	+23

Table S 1 Adsorption energies of Au and Cu atoms on non-hydrated, E_{ads}^{M/TiO_2}, and hydrated, $E_{ads}^{M/(nH_2O/TiO_2)}$, stoichiometric TiO_2 (110) surfaces (the nature of the metal M varying between Au and Cu, n being the number of dissociated water molecules on the surface). The hydration energies of the support in absence $E_{hyd}^{nH_2O/TiO_2}$ and presence of the metallic atom $E_{hyd}^{nH_2O/(M/TiO_2)}$ are addressed with the coadsorption energy between the metal and water on the various support surfaces $E_{coads}^{M,nH_2O/TiO_2}$, and the interaction energy between the metal and water through the support $E_{int}^{M-nH_2O}$. Two methods have been compared: all the DFT+U (UPBE+U) and DFT+U+D3 (UPBE+U+D3) energies are given in $kJ.mol^{-1}$.